

# Petrogenesis, oxidation state and volatile content of Dongga tonalite in the Gangdese belt, Xizang: Implication for porphyry Cu mineralization

Liqiang Zhang<sup>1,2</sup> · Xilian Chen<sup>1</sup> · Shaohao Zou<sup>1</sup> · Deru Xu<sup>2</sup> · Xuena Wang<sup>2</sup> · Hua Wang<sup>2</sup>

Received: 20 September 2023 / Revised: 3 November 2023 / Accepted: 30 November 2023 / Published online: 8 January 2024  
© The Author(s), under exclusive licence to Science Press and Institute of Geochemistry, CAS and Springer-Verlag GmbH Germany, part of Springer Nature 2024

**Abstract** The Gangdese belt in Xizang has experienced both Jurassic subduction and Cenozoic continental collision processes, making it a globally renowned region for magmatic rocks and porphyry copper deposits. Numerous Jurassic intrusions have been identified in the belt. Apart from the quartz diorite porphyry in the large Xietongmen deposit, the Cu mineralization potential of other Jurassic intrusions in this belt remains unclear. This study presents zircon U–Pb dating and trace elements, apatite major and trace elements as well as published whole-rock geochemical and isotopic data of the Dongga tonalite in the central part of the Gangdese belt, aiming to reveal the petrogenesis, oxidation state, volatile content, and Cu mineralization potential of this intrusion. The Dongga tonalite has a zircon U–Pb age of  $179.4 \pm 0.9$  Ma. It exhibits high whole-rock V/Sc values (8.76–14.6), relatively low apatite  $\text{Ce}_{\text{N}}/\text{Ce}_{\text{N}}^*$  ratios (1.04–1.28), elevated zircon ( $\text{Eu}/\text{Eu}^*$ )<sub>N</sub> values (an average of 0.44), high  $\text{Ce}^{4+}/\text{Ce}^{3+}$  values (205–1896), and high  $\Delta\text{FMQ}$  values (1.3–3.7), collectively suggesting a high magmatic oxygen fugacity. The Dongga tonalite features amphibole phenocrysts, relatively high whole-rock Sr/Y ratios (20.3–58.9), and lower zircon Ti temperatures

(502–740 °C), reflecting a high magmatic water content. Estimation of magmatic sulfur content (0.002–0.024 wt%) based on apatite  $\text{SO}_3$  contents indicates an enriched magma sulfur content. Combined with previous studies and the collected Sr–Nd–Hf isotopes, the Dongga tonalite is derived from juvenile lower crust related with subduction of the Neo-Tethys oceanic slab. When compared with Xietongmen ore-bearing porphyries, the Dongga tonalite exhibits remarkable similarities with the Xietongmen ore-bearing porphyries in terms of magma source, tectonic background, magmatic redox state, and volatile components, which indicates that the Dongga tonalite has a high porphyry Cu mineralization potential, and therefore, provides important guidance for the future mineralization exploration.

**Keywords** Tonalite · Zircon · Apatite · Mineralization potential · Dongga area · Gangdese belt

## 1 Introduction

Copper possesses excellent electrical conductivity, thermal conductivity, and malleability, making it widely utilized in traditional industries such as aerospace, steel, chemical, and medical sectors (Wen et al. 2008; Mo and Pan 2006; Guo et al. 2018). Additionally, it also plays a vital role in the development of emerging industries (Huang et al. 2019; Li et al. 2021; Wang et al. 2023). According to statistics, global copper demand is projected to reach 8 million tons by 2032 (Huang et al. 2019; Li et al. 2021; Wang et al. 2023). Despite being the world's largest consumer of copper, China's proven Cu reserves account for only 2.95% of the global copper reserves (Huang et al. 2019; Lebdioui 2020; Li et al. 2021; Benabdallah et al. 2023). Therefore, conducting research on the mineralization potential assessment for porphyry copper

**Supplementary Information** The online version contains supplementary material available at <https://doi.org/10.1007/s11631-023-00664-0>.

✉ Xilian Chen  
xilianchen@outlook.com

Deru Xu  
xuderu@gig.ac.cn

<sup>1</sup> State Key Laboratory of Nuclear Resources and Environment, East China University of Technology, Nanchang 330013, China

<sup>2</sup> School of Earth Sciences, East China University of Technology, Nanchang 330013, China

deposits could be a key to understanding mineralization process, and therefore could facilitate efficient exploration.

Porphyry deposits are the main source of copper and molybdenum, and a significant source of gold, providing approximately 75% of copper, 50% of molybdenum, and 20% of gold in the world (Wang et al. 2015a, 2015b; Xu et al. 2016; Huang et al. 2020). Consequently, they have become a primary target in modern mineral exploration efforts (Tang et al. 2015; Xu et al. 2021; Liu et al. 2022). The Gangdese metallogenic belt in Xizang is a globally renowned magmatic and porphyry copper belt. It has undergone the entire process from the subduction of the Neo-Tethyan oceanic plate to the collision between the Indian and Eurasian continental blocks. Over the past 50 years, remarkable advance has been made in post-collisional porphyry deposits, especially with the discovery of a series of giant and large collision-related porphyry Cu–Mo deposits, such as Qulong, Jiama, Tinggong, and Chongjiang (Wang et al. 2015a, 2015b; Xu et al. 2016; Chen et al. 2020a, 2020b; Huang et al. 2020; Zhao et al. 2022; Zhang et al. 2023). In contrast, porphyry Cu deposits formed related to the subduction of the Neo-Tethyan oceanic plate has received less attention due to only one large ore deposit (Xietongmen deposit) that have been found (Chen et al. 2020a, 2020b; Huang et al. 2020; Zhao et al. 2022; Zhang et al. 2023). The formation of porphyry Cu deposits is influenced by many factors such as the magmatic-hydrothermal system, composition of the parent magma, magma volume, magma viscosity, sulfide saturation, and timing of the fluid release (Hou et al. 2004; Xu et al. 2016; Lebdioui 2020; Wang et al. 2023). Previous studies have shown that ore-forming magmas of the porphyry Cu deposits usually exhibit characteristics of high oxygen fugacity, and high water-, sulfur-, and copper contents, which are key factors in determining the mineralization potential (Mao et al. 2017; Wu et al. 2017; Zhao et al. 2014, 2017a, 2017b; Guo et al. 2018; Zhu et al. 2022; Fan et al. 2022).

The Xietongmen porphyry Cu–Au deposit is the only known large Jurassic subduction-related porphyry Cu–Au deposit in the Gangdese Belt, south Xizang (Huang 2009; Lang 2007a, 2007b; Lang et al. 2012; Chen et al. 2020a, 2020b). According to previous studies, multiple coeval intermediate to felsic plutons are developed in the Gangdese Belt in the same tectonic settings (Wen et al. 2008; Zhao et al. 2009; Wang et al. 2015a, 2015b; Xu et al. 2016; Qu et al. 2022), raising the question of whether these coeval plutons also have the potential for subduction-related porphyry-type mineralization. Therefore, we present new geochronological, whole-rock geochemical, and mineralogical data for the tonalites in the Dongga area, Gangdese belt, and compare these data with the published data from the Xietongmen ore-bearing porphyry (Lang et al. 2010; Huang et al. 2011;

Tang et al. 2015; Wang et al. 2017; Yin et al. 2016; Xie et al. 2018), aiming to reveal whether the magmatic rock in the Dongga area has the potential for a porphyry copper deposit.

## 2 Regional geological background

The Xizang Plateau is divided into the Songpan–Ganze, Qiangtang, Lhasa, and Tethyan Himalayan terranes from north to south, which are separated by the Jinshajing, Bangong–Nujiang, and Indus–Yarlung Zangbo suture zones, respectively (Fig. 1a; Zhao et al. 2009, 2017a, 2017b; Wang et al. 2017; Guo et al. 2018; Zhang et al. 2022). The Lhasa terrane was further subdivided into northern, central, and southern subterrane, bounded by the Shiquan River–Nam Tso mélange Zone and the Luobadui–Milashan Fault, respectively (Zhang et al. 2005; Zhu et al. 2011).

The Gangdese Belt (Fig. 1b) located in the southern Lhasa terrane, is a globally renowned magmatic rocks and porphyry copper mineralization belt (Gao et al. 2016; Cai et al. 2019; Li et al. 2021; Xiao et al. 2021). The magmatic rocks within this belt formed as a result of Jurassic–Cretaceous subduction of Neo-Tethyan oceanic crust and the subsequent collision of Indian with Eurasian blocks during the Early Tertiary. Magmatic rocks are widely distributed along the southern margin of the Gangdese belt, including (1) Early Jurassic Yeba Formation volcanic rocks and Late Jurassic-Early Cretaceous Sangri Group volcanic rocks (Zhu et al. 2008). The former is mainly composed of basalt, andesite, dacite, and rhyolite, while the latter is dominated by basaltic andesite, andesite, and dacite (Zhu et al. 2009; Kang et al. 2014); (2) Triassic to Miocene Gangdese batholith, comprising gabbro, diorite, and granite (Wen et al. 2008; Guo et al. 2018); (3) Paleocene–Eocene co-collisional Linzizong volcanic rock series, including a variety of volcanic rocks ranging from andesite to rhyolite (Xu et al. 2016; Chen et al. 2021); (4) Miocene potassio-ultrapotassio volcanic rocks (Zhao et al. 2009; Hawkesworth et al. 2010) and adakitic intrusive rocks (Hou et al. 2004; Wu et al. 2017; Xu et al. 2020; Xiao et al. 2021). Complex structural deformation and fault zones are developed in the Gangdese belt, including thrust faults, strike-slip faults, and normal faults. The dominant orientation of these faults is predominantly east–west (Zhu et al. 2013; Wu et al. 2017; Mao et al. 2017; Guo et al. 2018; Cai et al. 2019; Tang et al. 2021; Xiao et al. 2021). The Gangdese Belt is host to numerous economically significant porphyry Cu–Mo deposits, primarily formed as a result of the collisions between the Indian and Eurasian continental blocks. Examples of these deposits include Qulong, Jiama, Chongjiang, Tinggong, Zhuno, and so on, which are classified as large- to giant-size porphyry Cu–Mo deposits. Additionally, only one large-size porphyry deposit

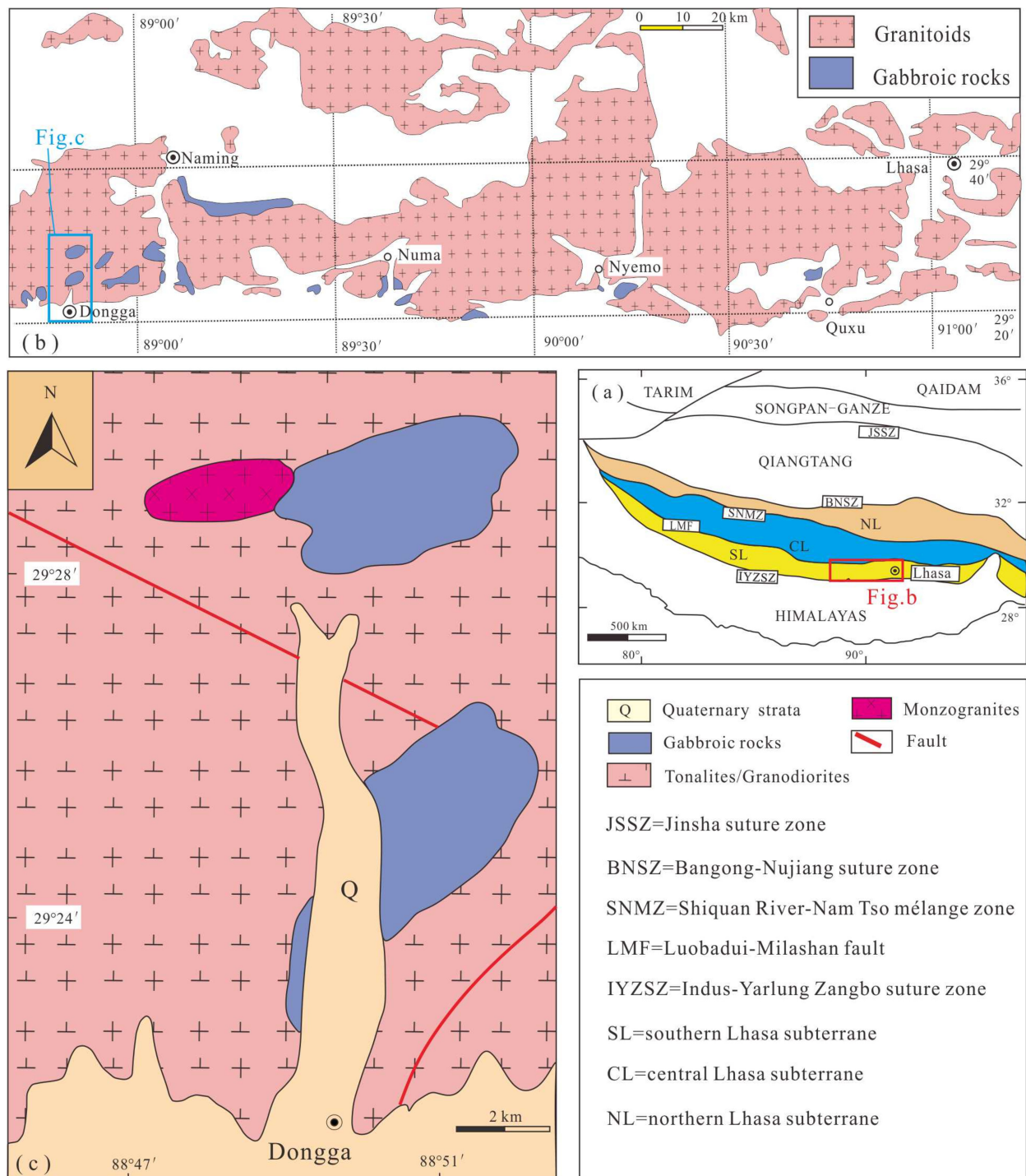


**Fig. 1** **a** Tectonic framework of the Xizang Plateau (modified after Zhu et al. 2011). **b** Simplified geological map of the southern Lhasa subterrane showing the distribution of the gabbro-granite complexes (modified after the 1:200 000 geological map). **c** Geological sketch map of the Dongga gabbro-granite complex (modified after the 1:200 000 geological map)

(modified after the 1:200 000 geological map). **c** Geological sketch map of the Dongga gabbro-granite complex (modified after the 1:200 000 geological map)

is associated with the subduction of the Neo-Tethys Ocean, namely the Xietongmen porphyry Cu–Au deposit.

The Xietongmen Cu–Au deposit is located in the Xietongmen County, southern Gangdese belt, Xizang (Lang

et al. 2010; Tang et al. 2012). The exposed strata in the mining area mainly consist of the Lower-Middle Jurassic Xiongcun Formation, which is primarily composed of volcanic breccia, volcanic conglomerate, and tuff, with

minor sandstone, siltstone, and shale. The magmatic rocks in the mining area were mainly formed during the Jurassic and Paleogene (Lang et al. 2010, 2012; Xie et al. 2015). Jurassic intrusive rocks include Early- to Mid-Jurassic hornblende-quartz diorite porphyry, Mid-Late Jurassic hornblende-quartz diorite porphyry with coarse-grained quartz phenocrysts, and Late Jurassic quartz diorite porphyry. Paleogene intrusive rocks consist of quartz diorite, biotite granite porphyry, and some pegmatite veins (Lang et al. 2012). The mining area is characterized by the development of fault structures, mainly brittle-ductile fault zones, and related fracture zones, which are distributed in a NW-, NWW-, and NE-trending (Lang et al. 2012; Tang et al. 2012). The alteration types in the district include potassic alteration, sericitization, and propylitic alteration. The primary ore bodies of the deposit are located in the contact zone between the quartz diorite porphyry and the volcanoclastic rocks of the Xiongcu Formation (Ding et al. 2012).

The study area is located in the Dongga area, near the city of Xigaze, north of the Yarlung Zangbo River, and is situated in the central Gangdese Belt (Fig. 1b, c). In the Dongga area, intrusive rocks are well-developed, with gabbro, tonalite, and granodiorite being the dominant rock types. The lithology of gabbro is mainly amphibolite gabbro, locally developed cumulate pyroxene. The surrounding rocks of gabbro are composed of tonalite and granodiorite, and the boundary between them is not obvious (Zhu et al. 2022). Some mafic enclaves (microgranular-fine-grained diorite or gabbro-diorite) are contained in these granitoids (Wang et al. 2017).

### 3 Petrographic characteristics

In this study, detailed field observation and microscopic examination were conducted on the petrography of the

tonalite in the Dongga area. The rock exhibits a mass structure, and its primary minerals include plagioclase (40–60 vol%), quartz (20–25 vol%), biotite (ca. 15 vol%) and hornblende (ca. 15 vol%) (Fig. 2a–c). The accessory minerals present in the rock include zircon, apatite, and titanite.

## 4 Analytical methods

### 4.1 Zircon U–Pb dating and trace element analysis

Zircon grains analyzed in this study were separated from samples using conventional heavy liquid and magnetic separation methods. They were handpicked under a binocular microscope and mounted in epoxy resin disks, which were then polished to expose the grains. Transmitted and reflected light micrographs and cathodoluminescence (CL) images were taken to characterize their internal structures. Zircon U–Pb dating and trace element analysis were conducted synchronously using laser ablation inductively-coupled plasma mass spectrometry (LA–ICP–MS) at the State Key Laboratory of Nuclear Resources and Environment, East China University of Technology, China. The zircon grains were then ablated for trace elements at the same spots using a Photon Machines Analyte NWR193HE excimer laser ablation system, coupled to an NexION 1000 quadrupole ICP–MS. Zircon grains were ablated using a 30  $\mu\text{m}$  diameter crater, the repetition rate of 8 Hz and 2.5 J/cm<sup>2</sup> fluence. All data were corrected by standard ZAF correction procedures. The obtained zircon U–Pb dating and trace element data were processed using Iolite software (Paton et al. 2011). The software Isoplot R (Vermeesch 2018) is used to calculate the weighted mean age and draw the Concordia diagrams (Appendices 1 and 2).

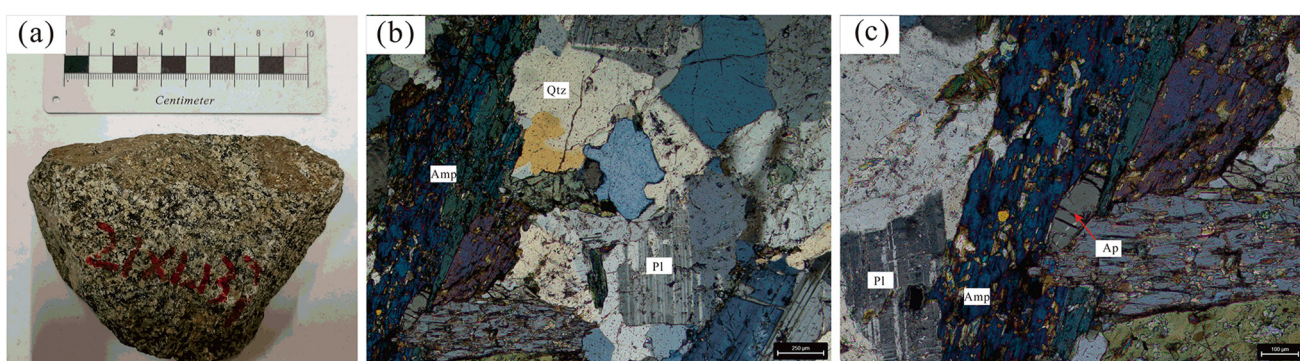


**Fig. 2** **a** Hand specimen photograph of tonalite in the Dongga area; **b, c** Micrographs of the tonalite. All the thin section photographs were taken under cross-polarized light. Qtz = Quartz; Amp = Amphibole; Ap = Apatite; Pl = Plagioclase

## 4.2 Apatite major element analysis

Apatite grains were separated from crushed rock samples through standard heavy-liquid and magnetic techniques. Then they were handpicked under a binocular microscope and mounted in epoxy resins. Apatite grains in this study are transparent and euhedral to subhedral in shape.

Apatite major element were determined using a FE-EPMA (JEOL JXA-8530F Plus) equipped with five wavelength-dispersive spectrometers at the State Key Laboratory of Nuclear Resources and Environment, East China University of Technology, China. The accelerating voltage, beam current and beam size were operated at 15 kV, 20 nA and 2–5  $\mu\text{m}$ , respectively. During the analysis routine, F and Cl were first analyzed to avoid their loss. The analytical uncertainties were < 1% for major elements. All raw data were corrected using the ZAF (atomic number, absorption, fluorescence) method (Appendix 3).

## 4.3 Apatite trace element analysis

Apatite trace elements were measured at the State Key Laboratory of Nuclear Resources and Environment, East China University of Technology, China. The mineral grains were ablated for trace elements at the same spots for the major element analyses using a Photon Machines Analyte NWR193HE excimer laser ablation system, coupled to an NexION 1000 quadrupole ICP-MS. A squid signal smoothing device is included in this laser ablation system. Apatite grains were ablated using a 30  $\mu\text{m}$  diameter crater, the repetition rate of 8 Hz and 2.5 J/cm<sup>2</sup> fluence. The apatite trace element results are given in Appendix 4.

## 5 Results

### 5.1 Zircon U–Pb dating

The zircon U–Pb data for the tonalite are in Appendix 1. Most zircon grains are mostly transparent, colorless to light yellow, euhedral crystals. These zircon grains are usually 150–250  $\mu\text{m}$  in length with 30–80  $\mu\text{m}$  in width. Additionally, zircon grains with low concordance (<90%) are removed. All zircon grains show oscillatory zoning in CL images and have Th/U ratios of 0.4–1.0 (Appendix 1), greater than 0.1, indicating these zircons are of magmatic origin (Schaltegger et al. 2005).

Twenty-nine zircon grains were analyzed for the tonalite. Eight zircon grains have a low concordance, which is excluded from the final average weighted mean age calculation. The other Twenty-one zircon grains yielded a weighted mean age of  $179.4 \pm 0.9$  Ma, with MSWD = 1.05 (Fig. 3).

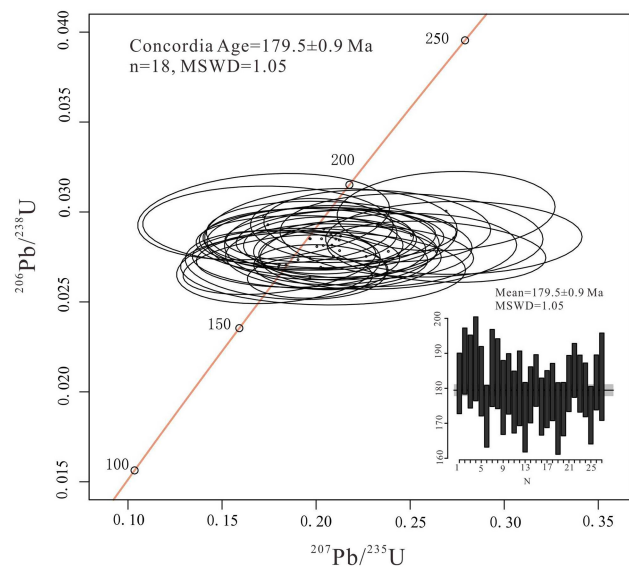


**Fig. 3** U–Pb concordia diagram of zircon grains from the tonalite in the Dongga area

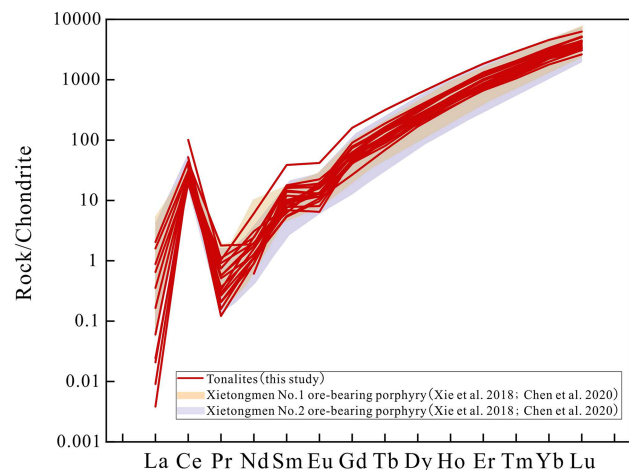


**Fig. 4** Distribution patterns of REE in zircons of the tonalite from the Dongga area and the Xietongmen ore-bearing porphyries. Normalization values for chondrite are taken from Sun and McDonough (1989)

### 5.2 Trace elements in zircons

To avoid the potential contamination from mineral inclusions like REE-bearing minerals and Ti-(Fe) oxides, zircon trace element data with La > 0.1 ppm and Ti > 50 ppm are filtered out. The zircon trace element results are shown in Appendix 2. The total rare earth element content ( $\sum\text{REE}$ ) ranges from 642 to 1134 ppm, with an average of 867 ppm (Appendix 2). Yttrium is highly enriched, ranging from 638 to 1332 ppm, with an average of 938 ppm. The rare earth element distribution pattern shows enrichment of heavy rare

earth elements (Gd–Lu) ranging from 586 to 1128 ppm and depletion of light rare earth elements (La–Eu) ranging from 13.9 to 36.5 ppm. The LREE/HREE ratios range from 0.020 to 0.037, with an average of 0.026, and  $(\text{Gd}/\text{Yb})_{\text{N}}$  shows a stable distribution with an average value of 0.025. In most samples, the average Ce content is 18.5 ppm, exhibiting a strong positive Ce anomaly. The  $(\text{Eu}/\text{Eu}^*)_{\text{N}}$  values range from 0.23 to 0.68, with an average of 0.44, indicating a negative Eu anomaly (Fig. 4). Using the zircon Ti thermometer method provided by Ferry and Watson (2007), the calculated zircon Ti temperatures range from 502 to 740 °C, with an average of 671 °C.

### 5.3 Apatite major and trace elements

The main components of apatite from the tonalites in the Dongga area are CaO,  $\text{P}_2\text{O}_5$ , F, MnO, and  $\text{SO}_3$ . The CaO and  $\text{P}_2\text{O}_5$  contents in the apatite are relatively homogeneous, with CaO ranging from 53.7 to 55.7 wt% (average of 54.7 wt%) and  $\text{P}_2\text{O}_5$  ranging from 40.4 to 42.7 wt% (average of 41.8 wt%) (Appendix 3). The  $\text{SO}_3$  content is between 0.18 and 1.11 wt% (average of 0.27 wt%). The apatites exhibit relatively high F content, ranging from 2.36 to 3.74 wt% (average of 2.93 wt%), while Cl content is relatively low, with a maximum value of 0.412 wt% and an average of 0.149 wt% (Appendix 3). There is a negative correlation between F and Cl elemental concentrations. In addition, the samples contain small amounts ( $\leq 1$  wt%) of  $\text{TiO}_2$ ,  $\text{K}_2\text{O}$ , FeO,  $\text{ThO}_2$ ,  $\text{Na}_2\text{O}$ , MgO,  $\text{Al}_2\text{O}_3$ , and  $\text{SiO}_2$ .

The trace element data of apatite from the tonalite in the Dongga area are provided in Appendix 4. Sr content in the apatites is relatively low, ranging from 284 to 765 ppm, with an average of 367 ppm. The apatites exhibit relatively high concentrations of rare earth elements (REE), with  $\Sigma\text{REE}$  ranging from 281 to 921 ppm and an average of 538 ppm. Yttrium is enriched, ranging from 248 to 547 ppm, with an average of 390 ppm. According to the rare earth element partitioning, LREE (La–Eu) ranges from 122 to 611 ppm, with an average of 296 ppm, and HREE (Gd–Lu) ranges from 156 to 332 ppm, with an average of 242 ppm. The ratios of LREE/HREE range from 0.61 to 3.2, with an average of 1.2, and the average  $(\text{Sm}/\text{Yb})_{\text{N}}$  ratio is 1.5, while the average  $(\text{La}/\text{Yb})_{\text{N}}$  ratio is 0.6. The apatite exhibits light rare earth element (LREE) depletion, heavy rare earth element (HREE) enrichment, negative Eu anomalies [ $(\text{Eu}/\text{Eu}^*)_{\text{N}} = 0.56\text{--}1.0$ ] and no significant Ce anomalies ( $\text{Ce}_{\text{N}}/\text{Ce}_{\text{N}}^* = 1.0\text{--}1.3$ ) (Fig. 5).

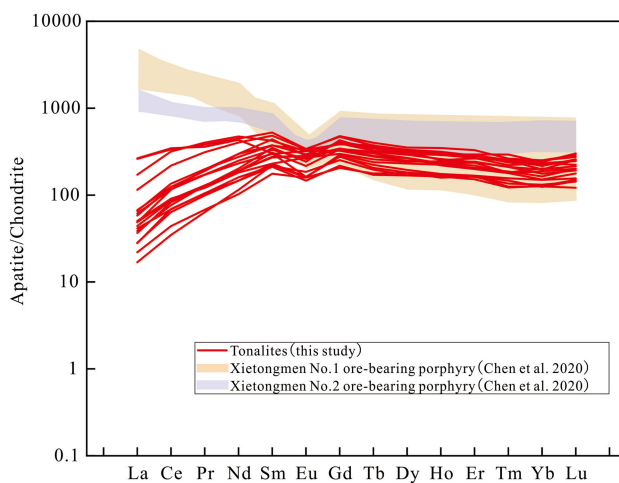


**Fig. 5** Apatite REE element patterns of the tonalite from the Dongga area and the Xietongmen ore-bearing porphyries (normalization values for chondrite are from Sun and McDonough 1989)

## 6 Collected whole-rock geochemical results

### 6.1 Whole-rock major elements

According to previous data (Appendix 5; Wang et al. 2017), this study provides a systematic summary of the major element compositions of the tonalite from the Dongga area. The tonalite from the Dongga area exhibits relatively low  $\text{SiO}_2$  content (56.7–62.7 wt%), moderate alkali content ( $\text{K}_2\text{O} + \text{Na}_2\text{O} = 5.28\text{--}5.69$  wt%), and low CaO content (5.65–7.14 wt%). The tonalite falls within diorite in the TAS diagram (Fig. 6a). The  $\text{Al}_2\text{O}_3$  content in the tonalite from the Dongga area is relatively low (16.4–18.4 wt%), and the A/CNK ratio ranges from 0.921 to 0.971. When plotted on the A/CNK-A/NK diagram, they fall within the sub-alkaline metaluminous field, indicating a typical metaluminous calc-alkaline nature (Fig. 6b, c). The  $\text{K}_2\text{O}$  content (1.33–1.48 wt%) and the AR content (1.54–1.66 wt%) are both relatively low (Fig. 6d), and when plotted on  $\text{SiO}_2\text{-K}_2\text{O}$  and AR- $\text{SiO}_2$  diagrams, the tonalite falls within the calc-alkaline series.

Summarizing the major element data of ore-bearing quartz diorite porphyries from the Xietongmen No. 1 and No. 2 deposits based on previous studies (Appendix 5; Lang et al. 2010; Huang et al. 2011; Yin et al. 2016; Chen et al. 2020a, b), the  $\text{SiO}_2$  content in the quartz diorite porphyries is relatively low, generally ranging from 61.4 to 68.2 wt%, while the alkali content is moderate, with  $\text{K}_2\text{O} + \text{Na}_2\text{O}$  ranging from 3.86 to 8.38 wt%. The dominant rock types of the quartz diorite porphyries fall within granodiorite in the TAS diagram (Fig. 6a), and the AR content is relatively low, ranging from 1.41 to 2.43 wt%. When plotted on the AR- $\text{SiO}_2$  diagram, the dominant rock types fall within

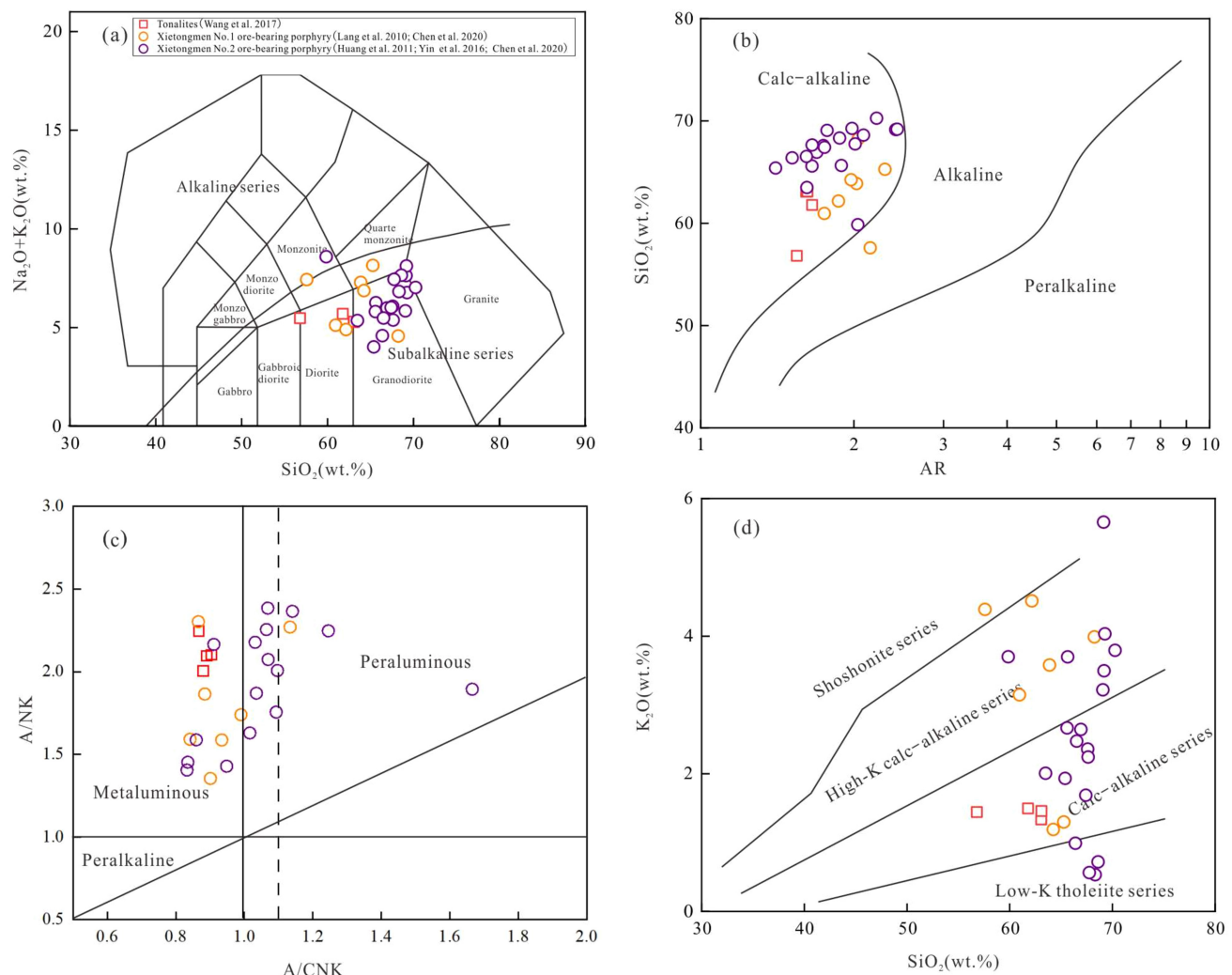


**Fig. 6** **a** Chemical classification diagram of  $\text{SiO}_2$ - $(\text{Na}_2\text{O} + \text{K}_2\text{O})$  [according to Middlemost (1994)]; **b** AR- $\text{SiO}_2$  diagram (according to Wright 1969); **c** A/CNK-A/NK diagram, (according to Irvine and

Baragar 1971, Maniar and Piccoli, 1989); and **d**  $\text{SiO}_2$ - $\text{K}_2\text{O}$  classification diagram for the tonalite from the Dongga area and the Xietongmen ore-bearing porphyries, according to Peccerillo and Taylor (1976)

the calc-alkaline series, indicating a calc-alkaline nature (Fig. 6b). The  $\text{Al}_2\text{O}_3$  content in the quartz diorite porphyries is relatively low, ranging from 13.1 to 19.7 wt%, and the A/CNK ratio ranges from 0.832 to 2.75. When plotted on the A/CNK-A/NK diagram, most of the samples fall within the sub-alkaline metaluminous and sub-alkaline weakly peraluminous fields (Fig. 6c).

## 6.2 Trace elements

According to previous studies (Appendix 5; Wang et al. 2017; Mahoney et al. 1998), this study provides a systematic summary of the trace element composition for the tonalite from the Dongga area. The tonalite from the Dongga area is enriched in elements such as K, Sr, and Pb, while depleted

in elements like Nb, Ta, Zr, and Hf (Fig. 7a). It exhibits relatively low total rare earth element ( $\Sigma\text{REEs}$ ) concentrations ranging from 50.2 to 65.6 ppm, indicating a light rare earth element-enriched pattern. The tonalite also displays positive Eu anomalies ( $\delta_{\text{Eu}} = 0.83\text{--}0.98$ ) (Fig. 7b).

Summarizing the trace element data of the Xietongmen No. 1 and No. 2 ore-bearing quartz diorite porphyries, based on previous studies (Appendix 5; Lang et al. 2010; Huang et al. 2011; Yin et al. 2016; Chen et al. 2020a, b), it is observed that the mineralized quartz diorite porphyries are characterized by enrichment in elements such as Rb, K, and Sr, while depletion in elements like Nb, Ta, and Ti (Fig. 7a). The total rare earth element ( $\Sigma\text{REEs}$ ) contents in the Xietongmen No. 1 and No. 2 quartz diorite porphyries are relatively low, ranging from 35.5 to 116 ppm, with

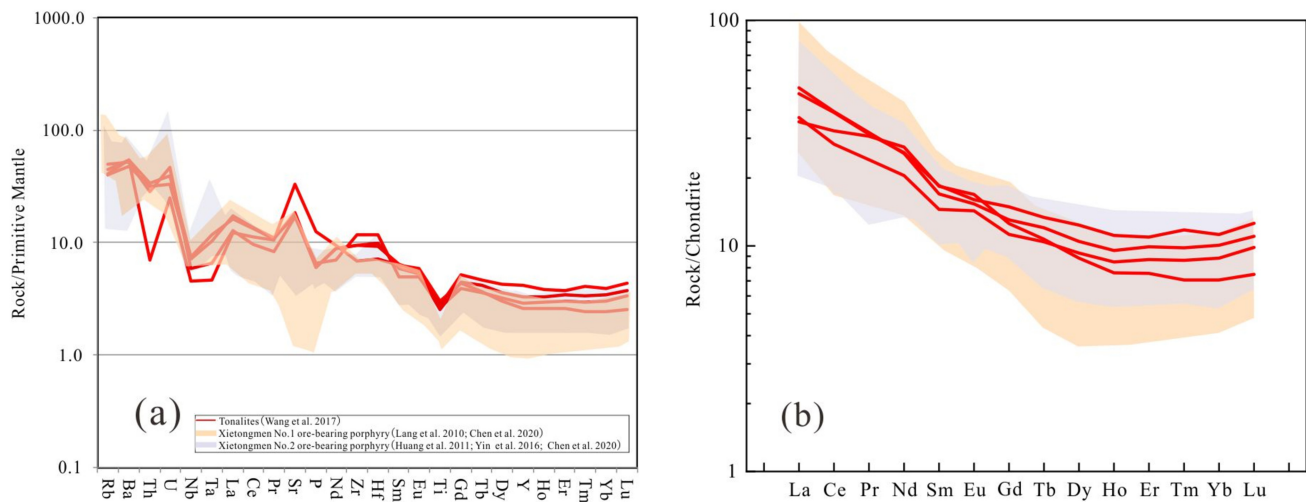


**Fig. 7** Primitive-mantle-normalized trace elements spider diagrams (a) and chondrite-normalized REE patterns (b) for the tonalite from the Dongga area and the Xietongmen ore-bearing porphyries (normalization values for chondrite are from Sun and McDonough 1989)

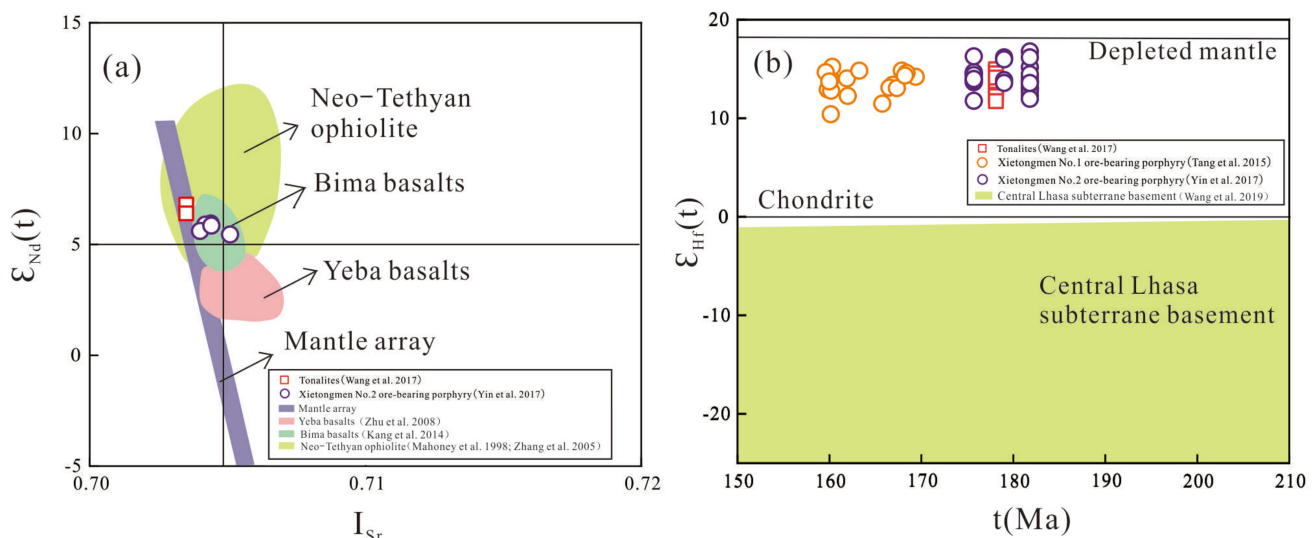


**Fig. 8**  $\epsilon_{\text{Nd}}(t)$ - $I_{\text{Sr}}$  diagram (a) and  $\epsilon_{\text{Hf}}(t)$ - $t$  diagram (b) of the tonalite from the Dongga area and the Xietongmen ore-bearing porphyries

(La/Yb)<sub>N</sub> ratios of 1.8–11. They exhibit relatively weak Eu anomalies ( $\delta_{\text{Eu}} = 0.64$ –1.3) (Fig. 7b).

### 6.3 Whole-rock Sr–Nd isotopes

This study provides a systematic summary of the whole-rock Sr–Nd isotope compositions of the tonalite from the Dongga area and the ore-bearing porphyries from the Xietongmen deposit based on Wang et al. (2017) and Yin et al. (2016) (Appendix 6). The tonalite from the Dongga area exhibits a limited range of Sr–Nd isotope compositions, with an initial  $^{87}\text{Sr}/^{86}\text{Sr}$  ratio ( $I_{\text{Sr}}$ ) of 0.7035. The  $\epsilon_{\text{Nd}}(t)$  values range

from 6.4 to 6.8. They possess young Nd model ages, with a  $T_{\text{DM2}}(\text{Nd})$  value ranging from 443 to 409 Ma (Fig. 8a).

For the Xietongmen ore-bearing porphyries, the  $I_{\text{Sr}}$  and  $\epsilon_{\text{Nd}}(t)$  values were calculated at a zircon U–Pb age of 179 Ma. The samples display relatively uniform initial  $^{87}\text{Sr}/^{86}\text{Sr}$  ratios ( $I_{\text{Sr}}$ ) ranging from 0.704 to 0.705, with an average of 0.704. The  $\epsilon_{\text{Nd}}(t)$  values range from 5.4 to 5.9. They also exhibit young Nd model ages, with Nd model ages [ $T_{\text{DM2}}(\text{Nd})$ ] ranging from 669 to 468 Ma (Fig. 8a).

#### 6.4 Zircon Hf isotopes

The Hf isotope composition of the tonalite from the Dongga area and the Xietongmen ore-bearing porphyries are collected, based on the previous studies (Tang et al. 2015; Wang et al. 2017; Yin et al. 2016; Appendix 7). The tonalite from the Dongga area exhibits highly depleted zircon Hf isotope compositions [ $\epsilon_{\text{Hf}}(t) = 11.4\text{--}15.0$ ] and also possesses young Hf model ages, with  $T_{\text{DM2}}(\text{Hf})$  values ranging from 493 to 262 Ma. The Xietongmen ore-bearing porphyries have  $\epsilon_{\text{Hf}}(t)$  values ranging from 10.4 to 16.8, with an average of 13.9, and the  $T_{\text{DM2}}(\text{Hf})$  values range from 515 to 119 Ma, with an average of 308 Ma (Fig. 8b).

### 7 Discussion

#### 7.1 Ages and tectonic setting

The obtained U–Pb dating result for the tonalite in the Dongga area of the Gangdese belt in this study is  $179.5 \pm 0.9$  Ma, indicating its formation in the Early Jurassic. This result is consistent with the previous study on the same rock in the Dongga area, which reported a similar age of  $179.7 \pm 1.7$  Ma (Wang et al. 2015a, b). By systematically collecting previous data on the ages of ore-bearing porphyries and mineralization in the Xietongmen deposit (Appendix 1, Chen et al. 2020a, b), it was found that the ages of quartz diorite porphyries in the Xietongmen No. 1 and No. 2 ore-bearing porphyries ( $166.3 \pm 2.6$  and  $175.5 \pm 1.0$  Ma, respectively) are consistent with the mineralization ages of the deposit (molybdenite Re–Os ages:  $161.5 \pm 2.7$  and  $172.6 \pm 2.1$  Ma, respectively).

The subduction of the Neo-Tethys Ocean is thought to be initiated at the Middle-Late Triassic (Wang et al. 2015a, b) or Early Jurassic (Zhang et al. 2015). During the Late Triassic to Cretaceous (230–80 Ma), the Neo-Tethys Oceanic slab underwent stable oblique subduction, triggering continuous magmatic activity in the Gangdese belt (Wang et al. 2015a). From the Early Cretaceous (~110 Ma), the subduction angle of the slab gradually increased, leading to an enhanced and southward migration of magmatic activity (Chen et al. 2020b; Guo et al. 2018). In the Cenozoic (~65 Ma), due to a steepening of the subduction angle, magmatic activity mainly concentrated along the southern margin of the Lhasa Terrane. Subsequently, around 50 Ma, a detachment occurred due to the collision between the Indian and Eurasian plates (Kang et al. 2014). Our data together with previous studies (Tang et al. 2015; Wang et al. 2017; Yin et al. 2016) indicate that the tonalite (with an age of  $179.5 \pm 0.9$  Ma) in the Dongga area and the Xietongmen ore-bearing porphyries ( $166.3 \pm 2.6$  and  $175.5 \pm 1.0$  Ma, respectively for the Xietongmen No. 1 and No. 2 ore-bearing porphyries)

in the Gangdese belt were formed in the Neo-Tethys Oceanic slab subduction process. Therefore, we conclude that the tonalites in the Dongga area and the Xietongmen ore-bearing porphyries have a similar formation age and tectonic background.

#### 7.2 Genetic types of rocks and source of magma

According to the mineral assemblage, whole-rock geochemical characteristics, and source properties, granite is commonly classified into I-type, S-type, and A-type granites (Chappell and White 1974; Whalen et al. 1987). I-type granites are primarily characterized by amphibole as the main indicative mineral, with accessory minerals such as magnetite, sphene, apatite, and zircon (Wu et al. 2017). The amphibole occurred as a major mineral in the tonalite. Besides, there are several distinguishing features between apatite in I-type granites and S-type granites. Firstly, in terms of source characteristics, I-type granites are derived from a mixture of mantle and lower crust (Barbarin et al. 1999; Chappell and White et al. 1974). While S-type granites are derived from partial melting of the lower crust. Secondly, apatite in I-type granites typically contains high amounts of F and Cl elements, while apatite in S-type granites is relatively depleted in these elements (Wu et al. 2017). This study demonstrates that the apatite in the tonalite in the Dongga area is rich in F and Cl elements. Additionally, The Sr–Nd/ $\text{Nd}^*$  isotopic composition of apatite also indicates that the tonalite in the Dongga area belongs to the I-type granite (Fig. 9), which is the same rock type as the Xietongmen ore-bearing porphyries (Chen et al. 2020a, b).

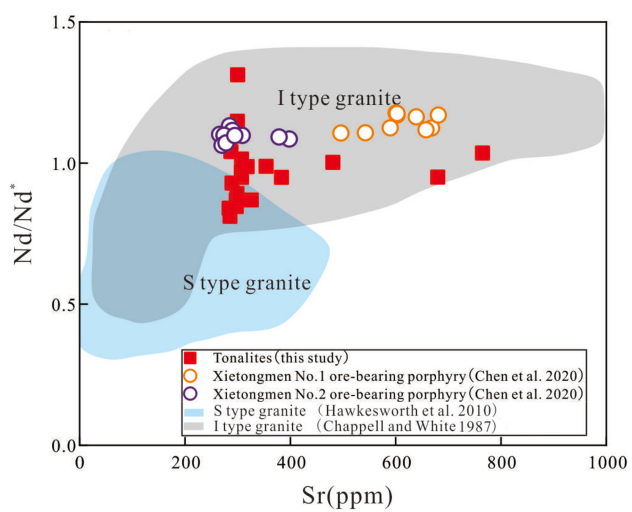


**Fig. 9** Apatite Sr–Nd/ $\text{Nd}^*$  ratio for the tonalite from the Dongga area and the Xietongmen ore-bearing porphyries (modified after Zhang 2020)

The composition of the magma source is an important factor influencing porphyry mineralization, where depleted mantle-derived materials can provide abundant ore-related elements such as Au, Cu, and S, and exhibit depleted Sr–Nd–Hf isotope characteristics (Hou et al. 2006). Recent studies revealed that the  $\varepsilon_{\text{Nd}}(t)$  values of the tonalite in the Dongga area range from 6.42 to 6.82, and the two-stage model ages ( $t_{\text{DM2}}$ ) range from 443 to 409 Ma (Tang et al. 2015; Wang et al. 2017; Yin et al. 2016), indicating that the magma may have been derived from partial melting of juvenile lower crust (Fig. 8a). Furthermore, the granitic intrusive rocks in the Dongga area have depleted zircon Hf isotopic compositions [ $\varepsilon_{\text{Hf}}(t)=11.4\text{--}15.0$ ], suggesting that they are products of partial melting of juvenile lower crust, similar to the isotopic composition of depleted mantle. This indicates that the magma source in the Dongga area is likely a juvenile crust with a similar isotopic composition to the depleted mantle, capable of providing abundant ore-related elements such as Au, Cu, and S for the formation of porphyry deposits (Fig. 8b).

### 7.3 Magma redox state and volatile contents

Magma oxidation state and volatile contents (including water, sulfur) are vital for the formation of porphyry Cu deposit (Peccerillo and Taylor 1976; Zhao 2012; Li et al. 2014; Tang et al. 2015; Wang et al. 2021; Xu et al. 2021; Huang et al. 2022). High oxygen fugacity can facilitate the decomposition of sulfides in the source region and increase the solubility of Cu and S (Ferry and Watson 2007; Hou and Yang 2009; Wang et al. 2021). High water content facilitates the magma rising to shallow depths, where fluid saturation occurs, followed by the unloading of Cu, resulting in the formation of porphyry Cu mineralization. Therefore, the magma oxidation state and volatile contents (including water and sulfur) are crucial for the formation of porphyry Cu deposits.

#### 7.3.1 Magma oxidation state

Zircon  $(\text{Eu}/\text{Eu}^*)_{\text{N}}$  and  $\text{Ce}^{4+}/\text{Ce}^{3+}$  ratios, whole-rock V/Sc ratios, apatite  $\text{Ce}_{\text{N}}/\text{Ce}_{\text{N}}^*$  could reflect the magma oxidation states (Xiao et al. 2021; Xie et al. 2018; Zhu et al. 2022). Ce and Eu exhibit variable valence states, and the abundance of Eu in zircon often reflects the redox conditions of the magma. The Eu anomaly is commonly expressed using  $(\text{Eu}/\text{Eu}^*)_{\text{N}}$ , where  $\text{Eu}^*=\sqrt{\text{Sm}_N \cdot \text{Gd}_N}$ . Based on this,  $(\text{Eu}/\text{Eu}^*)_{\text{N}}$  can be used as a criterion to assess the relative oxygen fugacity of the magma (Trail et al. 2012), and that the zircon  $(\text{Eu}/\text{Eu}^*)_{\text{N}}$  values increase with higher oxygen fugacity. In this study, zircon trace element data from the tonalites samples in the Dongga area, with an average  $(\text{Eu}/\text{Eu}^*)_{\text{N}}$  value of 0.44 (Appendix 4), showed negative Eu anomalies, which are

highly consistent with the REE patterns of the Xietongmen ore-bearing porphyry with zircon  $(\text{Eu}/\text{Eu}^*)_{\text{N}}$  ratios ranging from 0.33 to 0.77 (average of 0.49) (Chen et al. 2020a, b; Xie et al. 2018) (Fig. 10b).

Under relatively oxidizing conditions, Zr in zircon is typically present as  $\text{Zr}^{4+}$ , while Ce exists as  $\text{Ce}^{4+}$  (Hoskin and Schaltegger 2018). Due to the similar valence state and ion radius between  $\text{Ce}^{4+}$  and  $\text{Zr}^{4+}$ , Ce can easily substitute for  $\text{Zr}^{4+}$  in the zircon lattice, resulting in positive Ce anomalies. The  $\text{Ce}^{4+}/\text{Ce}^{3+}$  ratio in zircon can be used to reflect the oxygen fugacity of the magmatic system (Li et al. 2014; Huang et al. 2019). Zircon  $\text{Ce}^{4+}/\text{Ce}^{3+}$  values for the tonalite ranged from 205 to 1896, showing relatively high  $\text{Ce}^{4+}/\text{Ce}^{3+}$  values in this region (Appendix 2). By comparing with the data from Chen et al. (2020a, b) and Xie et al. (2018), it was found that the Xietongmen No. 1 and No. 2 ore-bearing porphyries have similar and relatively high zircon  $\text{Ce}^{4+}/\text{Ce}^{3+}$  values (respectively, ranging from 11.8 to 1745 and 10.9 to 4106) (Fig. 10c). Magmatic oxygen fugacity is proposed to be calculated using Ce, U, and Ti in zircon:  $\log fO_2(\text{samples}) - \log fO_2(\text{FMQ}) = 3.998(\pm 0.124) \times \log \left( \frac{\text{Ce}}{\sqrt{\text{U}_i \times \text{Ti}}} \right) + 2.284(\pm 0.101)$  (Loucks et al. 2020). Based on this formula, the tonalite in the Dongga area has  $\Delta\text{FMQ}$  values ranging from 1.3 to 3.7 (Appendix 2). The Xietongmen No. 1 and No. 2 ore-bearing porphyries has  $\Delta\text{FMQ}$  values of 0.56–1.8 and 0.73–1.83, respectively (Fig. 10d). The whole-rock V/Sc ratios can effectively reflect changes in magma oxygen fugacity. V and Sc exhibit similar geochemical behaviors during partial melting processes in the mantle (Canil 1997; Toplis and Corgne 2002).

At a given temperature, higher magma oxygen fugacity corresponds to larger V/Sc ratios, and subsequent weathering and metamorphism processes do not significantly impact the V/Sc ratio. Published data on the whole-rock V/Sc ratios of tonalite from the Dongga area and the Xietongmen ore-bearing porphyries support this observation (Lang et al. 2010; Huang et al. 2011; Wang et al. 2017; Yin et al. 2016; Chen et al. 2020a, 2020b). The whole-rock V/Sc ratios of the tonalite in the Dongga area (ranging from 8.76 to 14.6, with an average of 10.6) are very similar to those of Xietongmen ore-bearing porphyries (ranging from 6.64 to 22.3, with an average of 11.4) (Fig. 11). The Ce anomaly in apatite is also considered a representative of the oxidized state of the parental magma, as  $\text{Ce}^{3+}$  in apatite is more easily substituted compared to  $\text{Ce}^{4+}$  (Sha and Chappell 1999; Cao et al. 2012; Huang et al. 2023). Apatite crystals crystallized in relatively oxidized magmas will have lower  $\text{Ce}_{\text{N}}/\text{Ce}_{\text{N}}^*$  ratios compared to those crystallized in reduced magmas. In other words, higher magma oxygen fugacity corresponds to lower  $\text{Ce}_{\text{N}}/\text{Ce}_{\text{N}}^*$  ratios. The tonalite from the Dongga area exhibits relatively low apatite  $\text{Ce}_{\text{N}}/\text{Ce}_{\text{N}}^*$  ratios ranging from 1.04 to 1.28 (Appendix 4). Previous data analysis by Chen et al. (2020a, 2020b) also indicates that apatite from the Xietongmen ore-bearing porphyries has relatively

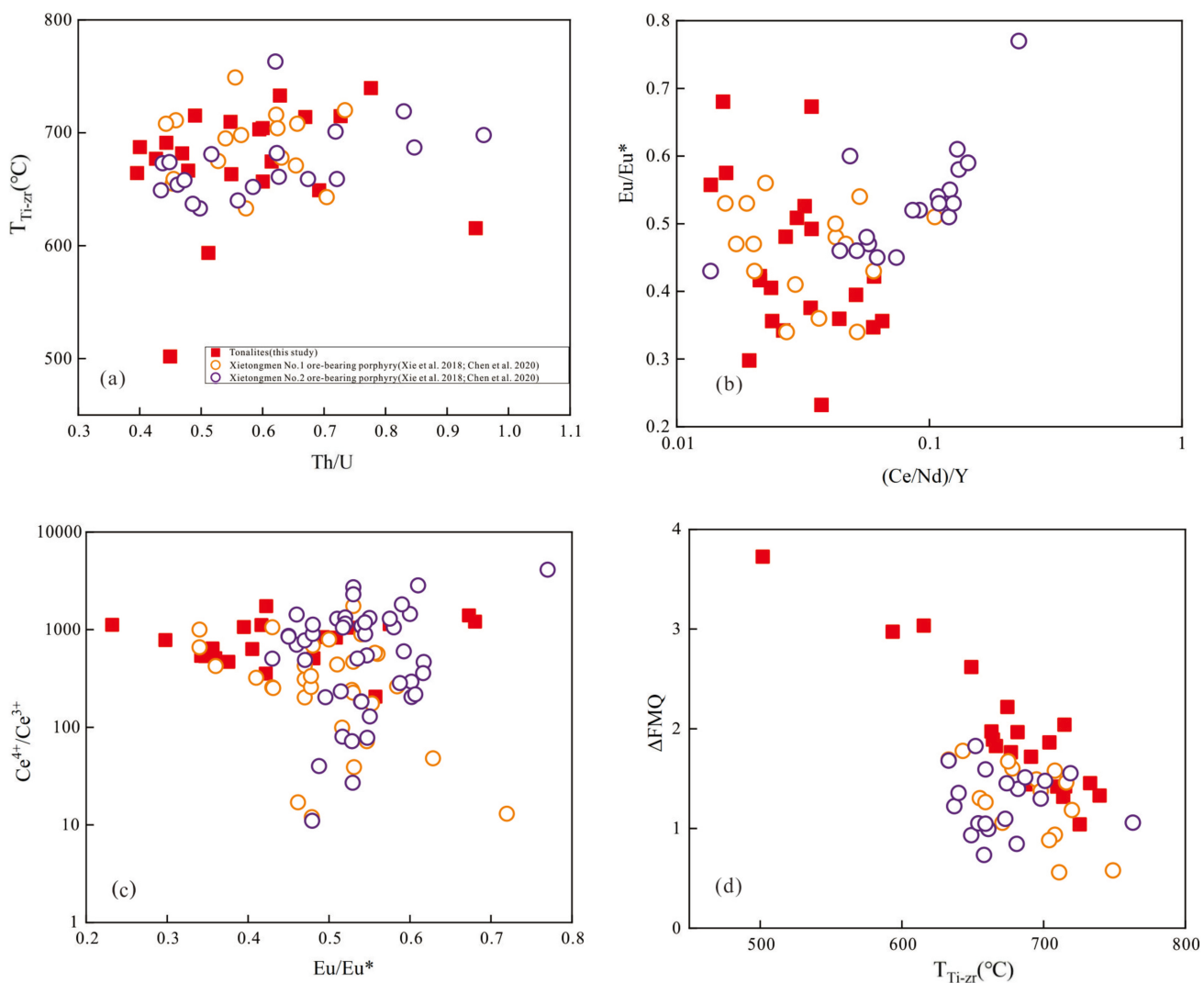


**Fig. 10** Diagrams for Ti-in-zircon temperature vs. Th/U (a), zircon (Ce/Nd)/Y versus Eu/Eu<sup>\*</sup> (b), zircon Eu/Eu<sup>\*</sup> vs. Ce<sup>4+</sup>/Ce<sup>3+</sup> (c), and zircon FMQ versus Ti-in-zircon temperature relationships (d)

low Ce<sub>N</sub>/Ce<sub>N</sub><sup>\*</sup> ratios (ranging from 0.97 to 1.0). The similarity in apatite Ce<sub>N</sub>/Ce<sub>N</sub><sup>\*</sup> ratios between the two regions suggests comparable oxygen fugacity conditions in the magmas of the Dongga area and the Xietongmen deposits (Fig. 12). These features indicate that the parental magma of the tonalite in the Dongga area is relatively oxidized, similar to those of the Xietongmen ore-bearing porphyries, favoring the formation of porphyry copper deposits.

### 7.3.2 Magma volatile contents

**Magma water content:** The occurrences of amphibole, relatively high whole-rock Sr/Y ratios, and low Ti-in-zircon temperature are important proxies for high magma water content (Piccoli and Candela 2002; Ding et al. 2012; Zhao 2012; Loucks et al. 2020; Wang et al. 2021). According to

our observations for the tonalite in the Dongga area, as well as previous studies on the Xietongmen ore-bearing porphyries (Chen et al. 2020a, b), all of these rock samples contain amphibole phenocrysts. The higher water content in the magma inhibits the separation crystallization of plagioclase, making amphibole the main segregate phase. Additionally, based on previous whole-rock geochemical data of the Dongga tonalite (Wang et al. 2017), these rocks exhibit relatively high whole-rock Sr/Y ratios ranging from 20.3 to 58.9, which are comparable to the Sr/Y ratios of the Xietongmen No. 1 and No. 2 ore-bearing porphyries (4.5 to 38.4 and 8.3 to 40.1, respectively) (Lang et al. 2010; Huang et al. 2011; Yin et al. 2016; Chen et al. 2020a, b) (Fig. 13). Furthermore, our study on tonalites samples reveals relatively low Ti-in-zircon temperatures, ranging from 502 to 740 °C with the average value of 671 °C. Ti-in-zircon temperatures

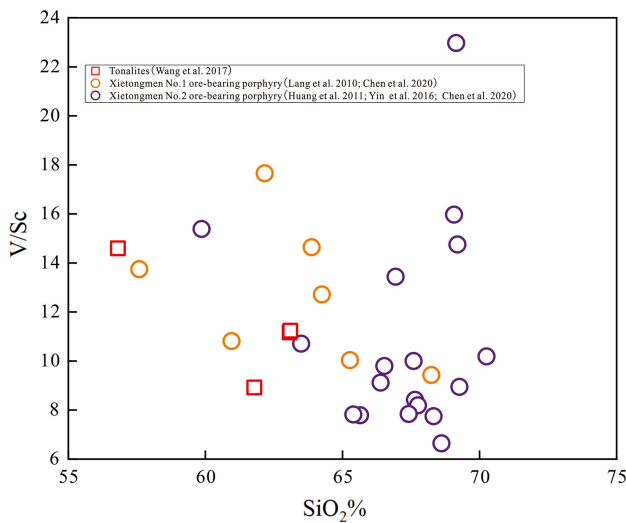


**Fig. 11** The V/Sc-SiO<sub>2</sub> diagram for the tonalite from the Dongga area and the Xietongmen ore-bearing porphyries

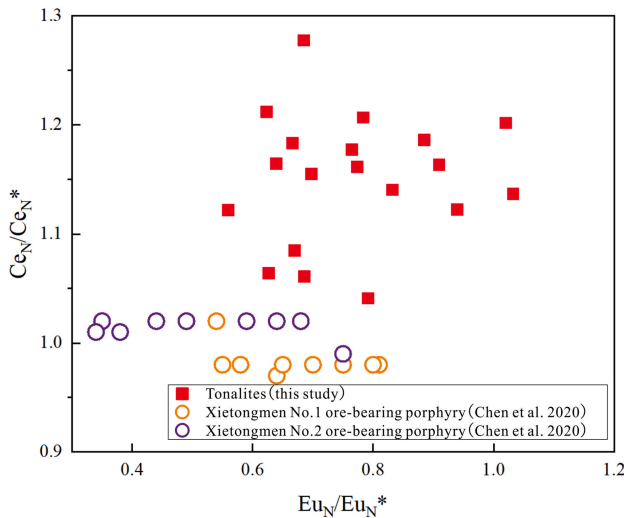


**Fig. 12** Apatite (Eu/Eu<sup>\*</sup>)<sub>N</sub>-Ce<sub>N</sub>/Ce<sub>N</sub><sup>\*</sup> diagram of the tonalite from the Dongga area and the Xietongmen ore-bearing porphyries

of the Xietongmen No. 1 and No. 2 ore-bearing porphyries are also relatively low, ranging from 607 to 763 °C with the average value of 672 °C, respectively (Xie et al. 2018; Chen et al. 2020a, b) (Fig. 10a). The presence of amphibole phenocrysts, relatively high whole-rock Sr/Y ratios, and low Ti-in-zircon temperatures for the tonalite in the Dongga area, similar to those for the Xietongmen ore-bearing porphyries, supports that these rocks were formed from water-rich magmas, favoring the formation of porphyry copper deposits.

Calculating magmatic sulfur contents based on the apatite SO<sub>3</sub> contents is complex, because that the apatite SO<sub>3</sub> contents are not only affected by magmatic sulfur contents, but also magma temperatures, and oxidation state (Peng et al.

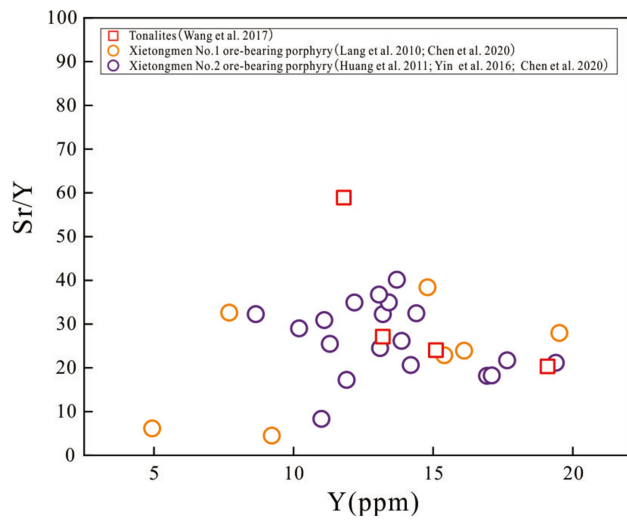


**Fig. 13** The Y-Sr/Y diagram for the tonalite from the Dongga area and the Xietongmen ore-bearing porphyries

1997; Belousova et al. 2002; Parat and Holtz 2005; Parat, Holtz and Streck 2011). Nevertheless, Peng et al. (1997) provided the apatite-melt partition coefficient formula of  $\ln K_d = \ln[(SO_3)_{ap}/(SO_3)_{melt}] = 21130/T - 16.2$ , which can be used to estimate magmatic S content semiquantitatively. The estimated magmatic S contents are 0.002–0.024 wt% for tonalite samples in the Dongga Area. Besides, previous studies proposed a partitioning relationship of  $(SO_3)_{ap} = 0.157 \times \ln(SO_3)_{melt} + 0.9834$  for magma sulfur content and apatite sulfur content (Parat, Holtz and Streck 2011). Estimation of magmatic S content based on the apatite saturation temperatures and the equation of Parat Holtz and Streck (2011) yields 0.001–0.043 wt% for tonalite samples in the Dongga Area. These values are comparable to the magmatic sulfur content of the Xietongmen No. 1 and No. 2 ore-bearing porphyries, which were calculated to be in the range of 0.011–0.051 wt% and 0.001–0.012 wt% using the formula of Peng et al. (1997), as well as 0.002–0.037 wt% and 0.001–0.026 wt% when employing the formula of Parat Holtz and Streck (2011). Therefore, the magmas of tonalite in the Dongga Area are sulfur-rich.

#### 7.4 Implication for porphyry copper mineralization

This study presents a systematic analysis of the petrology, whole-rock geochemistry, and mineralogy of the tonalite in the Dongga area, Gangdese belt. By integrating previous researches, the study proposes that the granitoids in the Dongga area may have the potential to form porphyry copper deposits. The main supporting evidence includes: (1) The tonalite in the Dongga area formed in Early Jurassic, and derived from partial melting of juvenile lower crust during the Neo-Tethyan oceanic plate subduction process. The

magmatic source in the area resembles the isotopic composition of the depleted mantle. This magmatic source is capable of supplying abundant ore-forming metal elements such as Au and Cu, as well as S elements, facilitating the formation of porphyry copper deposits. (2) The high oxidation state of magmas plays a crucial role in the formation of porphyry deposits. The tonalite exhibits the whole-rock V/Sc ratios ranging from 8.76 to 14.6 (average of 10.6), apatite  $\text{Ce}_{\text{N}}/\text{Ce}_{\text{N}}^*$  ranging from 1.04 to 1.28, average zircon ( $\text{Eu}/\text{Eu}^*$ )<sub>N</sub> of 0.44, and  $\text{Ce}^{4+}/\text{Ce}^{3+}$  ratios ranging from 205 to 4392,  $\Delta\text{FMQ}$  values ranging from 1.3 to 3.7. These characteristics indicate that the parental magmas of the tonalite in the Dongga area exhibit high oxygen fugacity, favoring the formation of porphyry deposits. (3) Volatile components such as S and water are essential media for magmatic-hydrothermal processes, facilitating the further enrichment of ore-forming elements. The presence of amphibole phenocrysts, relatively high whole-rock Sr/Y ratios (ranging from 20.3 to 58.9), and low Ti temperatures in zircon ranging from 502 to 740 °C (average value of 671 °C) for the tonalite in the Dongga area suggest a high magma water content. Besides, the magma is sulfur-rich as calculated based on the apatite  $\text{SO}_3$  contents (see Sect. 7.3). These characteristics suggest that the tonalite in the Dongga area are enriched in volatile components such as water and S, which promote the enrichment of ore-forming elements. By studying the magmatic source, tectonic background, redox state of magmas, and volatile components of the tonalites in Dongga area, and comparing them with the mineralized porphyry rocks of the Xietongmen deposit, the study finds significant similarities between the two areas. This indicates that the Dongga area may have the potential to host large-scale porphyry copper deposits. The only known subduction-related porphyry Cu–Au deposit (Xietongmen porphyry Cu–Au deposit) in the Gangdese belt is probably due to the subsequent erosion process and/or lack of exploration (Chen et al. 2020a, 2020b).

## 8 Conclusions

This study conducted systematic analyses including zircon U–Pb dating, zircon trace element, apatite major and trace element on the tonalite in the Dongga area, Gangdese Belt. Then comparing the obtained results with collected published data on the Xietongmen ore-bearing porphyries, the following conclusions were drawn:

1. The tonalite in the Dongga area is an I-type granite and formed at  $179.4 \pm 0.9$  Ma, indicating an Early Jurassic crystallization age.

2. The tonalite in the Dongga area predominantly originated from partial melting of juvenile lower crust related with the Neo-Tethys oceanic plate subduction.
3. The tonalite in the Dongga area exists high oxygen fugacity, water- and S-rich features.
4. The tonalite in the Dongga area shares similarities to the Xietongmen ore-bearing porphyries in terms of magma source, tectonic background, magma redox state, and volatile contents, which suggest that it has the potential for the formation of porphyry copper deposits.

**Acknowledgements** This study was supported by the National Natural Science Foundation Program of China (42102095, 42362013, 42363009), the Jiangxi Provincial Natural Science Foundation (20224BAB203036, 20224BAB213040, 20224ACB203008), and the Open Research Fund Program of State Key Laboratory of Nuclear Resources and Environment, East China University of Technology (2022NRE12). We are grateful to Drs. Bin Wu and Kaixuan Li from the State Key Laboratory of Nuclear Resources and Environment, East China University of Technology, for their technical assistance in the process of EPMA analysis. Dr. Yan Zhao is thanked for guiding us during the zircon U–Pb dating and mineral trace elements analyses.

## References

- Barbarin B (1999) A review of the relationships between granitoid types their origins and their geodynamic environments. *Lithos*. 46(3): 605–626.
- Belousova EA, Griffin WL, O'Reilly SY, Fisher NI (2002) Apatite as an indicator mineral for mineral exploration: trace-element compositions and their relationship to host rock type. *J Geochem Explor*. 76(1):45–69.
- Benabdallah N, Luo D, Hadj Youcef M, Lopez J, Fernández de Labastida M, Sastre AM, Valderrama CA, Cortina JL (2023) Increasing the circularity of the copper metallurgical industry: Recovery of Sb(III) and Bi(III) from hydrochloric solutions by integration of solvating organophosphorous extractants and selective precipitation. *Chem Eng J*. 453:139811.
- Cai W, Wang Z, Li J, Fu L, Wang K, Konare Y, Li S (2019) Zircon U–Pb and molybdenite Re–Os geochronology and geochemistry of Jinchang porphyry gold–copper deposit, NE China: two-phase mineralization and the tectonic setting. *Ore Geol Rev*. 107:735–753.
- Canil D (1997) Vanadium partitioning and the oxidation state of Archaean komatiite magmas. *Nature*. 389:6653.
- Cao MJ, Li GM, Qin KZ, Seitmuratova EY, Liu YS (2012) Major and trace element characteristics of apatites in granitoids from Central Kazakhstan: Implications for petrogenesis and mineralization. *Resour Geol*. 62:63–83.
- Chappell B, White A (2001) Two contrasting granite types: 25 years later. *Australian J of Earth Sci*. 48(4): 489–499.
- Chen XL, Liang HY, Zhang J, Sotiriou P, Huang WT, Ren L, Zhang L and Zou YQ (2019) Geochemical characteristics and magma fertility for the Jurassic arc rocks in the Gangdese belt, Tibet. *Ore Geology Reviews*. 115:103169.
- Chen XL, Liang H, Zhang J, Huang W, Ren L, Zou Y (2020a) Geochemical characteristics and oxidation states of the Xietongmen ore-bearing porphyries: Implication for the genetic types of the Xietongmen No. I and No. II deposits, southern Tibet. *Geol J*. 55(6):4691–4712.

- Chen XL, Zheng Y, Gao S, Wu S, Jiang X, Jiang J, Cai P, Lin C (2020b) Ages and petrogenesis of the Late Triassic andesitic rocks at the Luerma porphyry Cu deposit, western Gangdese, and implications for regional metallogeny. *Gondwana Res.* 85:103–123.
- Chen XL, Leng CB, Zou SH, Li K, Zhang L (2021) Geochemical compositions of apatites from the Xuejiping and Disuga porphyries in Zhongdian arc: Implications for porphyry Cu mineralization. *Ore Geol Rev.* 130:103954.
- Ding F, Lang XH, Hu ZH, Yang HH, Wang ZZ, Zhang L (2012) The genesis of mineralized tuff of No. I Ore Body in the Xiongcuon Porphyry Copper-Gold Metallogenic Ore District, Tibet: evidence from geochemistry and Sr-Nd-Pb isotopes. *Acta Geoscientica Sinica*. 4:546–558 (in Chinese with English abstract).
- Fan FP, Xiao F, Chen SZ, Xing GF, Zhou Y, Chen F (2022) LA-ICP-MS zircon U-Pb dating of granite porphyry and  $^{40}\text{Ar}/^{39}\text{Ar}$  dating of chromian sericite of the Shuangqishan and Xiaoban gold deposits in central Fujian, South China and their restriction on gold mineralization. *Ore Geol Rev.* 148:105027.
- Ferry JM, Watson EB (2007) New thermodynamic models and revised calibrations for the Ti-in-zircon and Zr-in-rutile thermometers. *Contrib Miner Petrol.* 154:429–437.
- Gao Y, Mao JW, Ye HS, Li YF, Luo ZZ, Yang ZQ (2016) Petrogenesis of ore-bearing porphyry from the Tangjiaping porphyry Mo deposit, Dabie orogen: Zircon U-Pb geochronology, geochemistry and Sr-Nd-Hf isotopic constraints. *Ore Geol Rev.* 79:288–300.
- Guo W, Zeng Q, Zhang B, Hu Y (2018) Genesis of the Jurassic Dongfengbeishan porphyry Mo deposit in Eastern Yanbian, NE China inferred from molybdenite Re-Os and zircon U-Pb ages, and whole-rock elemental and zircon Hf isotopic compositions. *J Asian Earth Sci.* 165:256–269.
- Hawkesworth CJ, Dhuime B, Pietranik AB, Cawood PA, Kemp AIS (2010) The generation and evolution of the continental crust. *J Geol Soc Lond.* 167:229–248.
- Hoskin PW, Schaltegger U (2018) The composition of zircon and igneous and metamorphic petrogenesis. In: *Zircon* 165:27–62.
- Hou ZQ, Yang ZM (2009) Porphyry deposits in continental settings of China: geological characteristics, magmatic hydrothermal system, and metallogenic model. *Acta Geol Sin.* 83(12):1779–1817 (in Chinese with English abstract).
- Hou ZQ, Gao YF, Qu XM, Rui ZY, Mo XX (2004) Origin of adakitic intrusives generated during mid-Miocene east–west extension in southern Tibet. *Earth Planet Sci Lett.* 220(1):139–155.
- Hou ZQ, Yang ZS, Xu WY, Mo XX, Ding L, Gao YF (2006) Metallogenesis in Tibetan collisional orogenic belt: I. Mineralization in main collisional orogenic setting. *Miner Depos.* 25(4):337–358 (in Chinese with English abstract).
- Huang Y (2009) The geochemistry characteristics of xiongcuon copper-gold deposit, Xietongmen County, Tibet, China. Master's, Chengdu Univ Technol. 74:1022265 (in Chinese with English abstract).
- Huang Y, Tang JX, Lang XH, Zhang L (2011) Geochemical and chemical characteristics of intrusive rock-volcanic rocks of No 2 orebody in xiongcuon copper-gold deposit: constraints on rock genesis and tectonic setting. *Miner Depos.* 8(4):1456–1752 (in Chinese with English abstract).
- Huang ML, Bi XW, Gao JF, Xu LL, Xiao JF, Liu ST, Wang XS, Zhou T (2019) Sulfur and lead isotopic variations in the giant Yulong porphyry Cu (Mo Au) deposit from the eastern Tibetan Plateau: Implications for origins of S and Pb, and metal precipitation. *J Geochem Explor.* 197:70–83.
- Huang W, Liang H, Zhang J, Chen X, Shuping L, Zou Y, Ren L, Wu J, Zhang L (2020) Formation of the Cretaceous skarn Cu–Au deposits of the southern Gangdese belt, Tibet: case studies of the Kelu and Sangbujiala deposits. *Ore Geol Rev.* 122:103481.
- Huang ML, Zhu JJ, Bi XW, Xu LL, Xu Y (2022) Low magmatic Cl contents in giant porphyry Cu deposits caused by early fluid exsolution: a case study of the Yulong belt and implication for exploration. *Ore Geol Rev.* 220(200–201):157–168.
- Huang ML, Zhu JJ, Chiaradia M, Hu R, Xu L (2023) Apatite volatile contents of porphyry Cu deposits controlled by depth-related fluid exsolution processes. *Econ Geol.* 220(1):139–155.
- Irvine TN, Baragar WRA (1971) A guide to the chemical classification of the common volcanic rocks. *Can J Earth Sci.* 8(5):523–548.
- Kang ZQ, Xu JF, Wilde SA, Feng ZH, Chen JL, Wang BD, Fu WC, Pan HB (2014) Geochronology and geochemistry of the Sangri Group Volcanic Rocks, Southern Lhasa Terrane: implications for the early subduction history of the Neo-Tethys and Gangdese Magmatic Arc. *Lithos.* 200–201:157–168.
- Lang XH (2007a) Comparative study of xiongcuon copper-gold deposit and Dongga gold deposit in Tibet. Master's, Chengdu Univ Technol. 7(2):1341–1352 (in Chinese with English abstract).
- Lang XH, Tang JX, Chen YC, Li ZJ, Huang Y, Wang CY (2010) Re–Os geochronology and geological significance of molybdenite in No. 2 orebody of xiongcuon porphyry copper-gold deposit concentration area, Xietongmen County, Tibet. *Miner Rock.* 30(4):55–61 (in Chinese with English abstract).
- Lang XH, Tang JX, Li ZJ, Dong SY, Ding F, Wang ZZ, Zhang L (2012) A geochemistry assessment of the prospecting potential in and around xiongcuon copper-gold deposit, Xietongmen County, Tibet, China. *Geol Explor.* 48(1):12–23 (in Chinese with English abstract).
- Lang XH, Tang JX, Li ZJ, Huang Y, Ding F (2014) U-Pb and Re–Os geochronological evidence for the Jurassic porphyry metallogenic event of the Xiongcuon district in the Gangdese porphyry copper belt, southern Tibet, PRC. *J Asian Earth Sci.* 79:608–622.
- Lang XH (2007) Metallogenesis and metallogenic prognosis of porphyry copper-gold deposit in xiongcuon, Tibet. Master's, Chengdu University of Technology. Ph.d thesis, Chengdu University of Technology. 63:899–918 (in Chinese with English abstract).
- Lebdouli A (2020) Local content in extractive industries: Evidence and lessons from Chile's copper sector and Malaysia's petroleum sector. *Extr Ind Soc.* 7(2):341–352.
- Li GM, Cao MJ, Qin KZ, Evans NJ, McInnes BI, Liu YS (2014) Thermal-tectonic history of the Baogutu porphyry Cu deposit, West Junggar as constrained from zircon U-Pb, biotite Ar/Ar and zircon/apatite (U-Th)/He dating. *J Asian Earth Sci.* 79:741–758.
- Li B, Li H, Dong Z, Lu Y, Liu N, Hao X (2021) The global copper material trade network and risk evaluation: a industry chain perspective. *Resour Policy.* 74:102275.
- Liu P, Wu S, Zheng Y, Wang X, Kang Y, Yan J, Gu Y, Liu X, Gong F, Zhao Y, Ci Q, Chen L (2022) Geology and factors controlling the formation of the newly discovered Beimulang porphyry Cu deposit in the western Gangdese, southern Tibet. *Ore Geol Rev.* 144:104823.
- Loucks RR, Fiorentini ML, Henríquez GJ (2020) New magmatic oxygen barometer using trace elements in zircon. *J Petrol.* 61(3):034.
- Mahoney JJ, Frei R, Tejada MLG, Mo XX (1998) Tracing the Indian Ocean mantle domain through time: isotopic results from old West Indian, East Tethyan, and South Pacific Seafloor. *J Petrol.* 39:1285–1306.
- Maniar PD, Piccoli PM (1989) Tectonic discrimination of granitoids. *Geol Soc Am Bull.* 101(5):635–643.
- Mao J, Xiong B, Liu J, Pirajno F, Cheng Y, Ye H, Song S, Dai P (2017) Molybdenite Re/Os dating, zircon U-Pb age and geochemistry of granitoids in the Yangchuling porphyry W-Mo deposit (Jiangnan tungsten ore belt), China: Implications for petrogenesis, mineralization and geodynamic setting. *Lithos.* 286–287:35–52.
- Middlemost EAK (1994) Naming materials in the magma/igneous rock system. *Earth Sci Rev.* 37(3):215–224.

- Mo XX, Pan GT (2006) Formation from Tethys to the Tibetan Plateau: constraints of tectonic-magmatic events. *Front Geol.* 6:43–51 (**in Chinese with English abstract**).
- Parat F, Holtz F (2005) Sulfur partition coefficient between apatite and rhyolite: the role of bulk S content. *Contributions to Mineralogy and Petrology*. 150(6): 643–651.
- Parat F, Holtz F and Streck MJ (2011) Sulfur-bearing magmatic accessory. *Minerals Reviews in Mineralogy and Geochemistry*. 73(1): 285–314.
- Parat F, Holtz F and Streck MJ (2011) S-rich apatite-hosted glass inclusions in xenoliths from La Palma: constraints on the volatile partitioning in evolved alkaline magmas. *Contrib Miner Petrol* 162:463–478.
- Paton C, Hellstrom J, Paul B, Woodhead J, Hergt J (2011) Iolite: Free-ware for the visualisation and processing of mass spectrometric data. *J Anal at Spectrom.* 26(12):2508–2518.
- Peccerillo A, Taylor SR (1976) Geochemistry of eocene calc-alkaline volcanic rocks from the Kastamonu area, Northern Turkey. *Contrib Miner Petrol.* 58(1):63–81.
- Peng G, Luhr JF, McGee JJ (1997) Factors controlling sulfur concentrations in volcanic apatite. *Am Miner.* 82(11–12):1210–1224.
- Piccoli PM, Candela PA (2002) Apatite in igneous systems. *Rev Miner Geochem.* 48(1):255–292.
- Qu P, Niu HC, Weng Q, Yang WB, Yang YY, Zhang D (2022) *In-situ* U–Pb geochronology, elemental and Nd isotopic compositions of titanite from the Mesozoic porphyry Mo deposits, NE China. *Ore Geol Rev.* 144:104817.
- Schaltegger U, Pettke T, Audétat A, Reusser E, Heinrich CA (2005) Magmatic-to-hydrothermal crystallization in the W–Sn mineralized Mole Granite (NSW, Australia): part I: crystallization of zircon and REE-phosphates over three million years—a geochemical and U–Pb geochronological study. *Chem Geol.* 220(3):215–235.
- Sha LK, Chappell BW (1999) Apatite chemical composition, determined by electron microprobe and laser-ablation inductively coupled plasma mass spectrometry, as a probe into granite petrogenesis. *Geochim Cosmochim Acta.* 63(22):3861–3881.
- Sun SS, McDonough WS (1989) Chemical and isotopic systematics of oceanic basalts: implications for mantle composition and processes. *Geological Society London Special Publications.* 42(1): 313–345.
- Tang JX, Dor J, Liu HF, Lang XH, Zhang JS, Zheng WB, Ying LJ (2012) Minerogenetic series of ore deposits in the east part of the Gangdise metallogenic belt. *Acta Geosci Sin.* 33(4):393–410 (**in Chinese with English abstract**).
- Tang JX, Lang X, Xie F, Gao Y, Li Z, Huang Y, Ding F, Yang H, Zhang L, Wang Q, Zhou Y (2015) Geological characteristics and genesis of the Jurassic No. I porphyry Cu–Au deposit in the Xiongcuo district, Gangdise porphyry copper belt, Tibet. *Ore Geol Rev.* 70:438–456.
- Tang P, Tang J, Wang Y, Lin B, Leng Q, Zhang Q, He L, Zhang Z, Sun M, Wu C, Qi J, Li Y, Dai S (2021) Genesis of the Lakang'e porphyry Mo (Cu) deposit, Tibet: constraints from geochemistry, geochronology, Sr–Nd–Pb–Hf isotopes, zircon and apatite. *Lithos.* 380–381:105834.
- Toplis MJ, Corgne A (2002) An experimental study of element partitioning between magnetite, clinopyroxene and iron-bearing silicate liquids with particular emphasis on vanadium. *Contrib Miner Petrol.* 144(1):22–37.
- Trail D, Bruce Watson E, Tailby ND (2012) Ce and Eu anomalies in zircon as proxies for the oxidation state of magmas. *Geochim Cosmochim Acta.* 97:70–87.
- Vermeesch P (2018) IsoplotR: a free and open toolbox for geochronology. *Geosci Front.* 9:1479–1493.
- Wang R, Richards JP, Zhou L, Hou Z, Stern RA, Creaser RA, Zhu J (2015a) The role of Indian and Tibetan lithosphere in spatial distribution of Cenozoic magmatism and porphyry Cu–Mo deposits in the Gangdese belt, southern Tibet. *Earth Sci Rev.* 150:68–94.
- Wang Q, Zhu DC, Cawood PA, Zhao ZD, Liu SA, Chung S-L, Zhang LL, Liu D (2015b) Eocene magmatic processes and crustal thickening in southern Tibet: Insights from strongly fractionated ca. 43 Ma granites in the western Gangdese Batholith. *Lithos.* 239:128–141.
- Wang RQ, Qiu JS, Yu SB, Zhao JL (2017) Crust–mantle interaction during Early Jurassic subduction of Neo–Tethyan oceanic slab: evidence from the Dongga gabbro–granite complex in the southern Lhasa subterrane, Tibet. *Lithos.* 292–293:262–277.
- Wang R, Luo HC, Xia WJ, Sun YC, Liu B (2021) Advances in research on the genesis of high-water, high-oxygen fugacity magmas in the gangdise post-collisional porphyry metallogenic belt. *Miner Rock Geochem.* 40(5):1061–1077997 (**in Chinese with English abstract**).
- Wang J, Liu W, Chen L, Li X, Wen Z (2023) Analysis of China's non-ferrous metals industry's path to peak carbon: a whole life cycle industry chain based on copper. *Sci Total Environ.* 892:164454.
- Wen DR, Chung SL, Song B, Iizuka Y, Yang HJ, Ji J, Liu D, Gallet S (2008) Late Cretaceous Gangdese intrusions of adakitic geochemical characteristics, SE Tibet: Petrogenesis and tectonic implications. *Lithos.* 105(1):1–11.
- Whalen J, Currie K, Chappell B (1987) A-type granites: Geochemical characteristics, discrimination and petrogenesis. *Contrib Miner Petrol.* 95:407–419.
- Wright JB (1969) A simple alkalinity ratio and its application to questions of non-orogenic granite genesis. *SUMMARY Geological Magazine.* 106(4): 370–384.
- Wu YS, Zhou KF, Li N, Chen YJ (2017) Zircon U–Pb dating and Sr–Nd–Pb–Hf isotopes of the ore-associated porphyry at the giant Donggebi Mo deposit, Eastern Tianshan, NW China. *Ore Geol Rev.* 81:794–807.
- Xiao X, Zhou T, White NC, Fan Y, Zhang L, Chen X (2021) Porphyry Cu mineralization processes of Xinqiao deposit, Tongling ore district: constraints from the geochronology and geochemistry of zircon, apatite, and rutile. *Ore Geol Rev.* 138:104340.
- Xie FW, Tang JX, Lang XH (2015) Study on ore-bearing of Porphyry of No 1. orebody in Xiongcuo mining area, Tibe—evidence from hydrothermal alteration minerals and accessory minerals. *J Rock Mineral.* 34(1):51–64 (**in Chinese with English abstract**).
- Xie FW, Tang JX, Chen Y, Lang XH (2018) Apatite and zircon geochemistry of Jurassic porphyries in the Xiongcuo district, southern Gangdese porphyry copper belt: Implications for petrogenesis and mineralization. *Ore Geol Rev.* 96:98–114.
- Xu YG, Huang XL, Ma JL, Wang YB, Iizuka Y, Xu JF, Wang Q, Wu XY (2004) Crust–mantle interaction during the tectono-thermal reactivation of the North China Craton: constraints from SHRIMP zircon U–Pb chronology and geochemistry of Mesozoic plutons from western Shandong. *Contrib Miner Petrol.* 147:750–767.
- Xu J, Zheng Y, Sun X, Shen Y (2016) Geochronology and petrogenesis of Miocene granitic intrusions related to the Zhibula Cu skarn deposit in the Gangdese belt, southern Tibet. *J Asian Earth Sci.* 120:100–116.
- Xu Q, Zeng LS, Gao JH, Gao LE, Wang YF, Hu ZP, Zhao LH (2019) The geochemistry characteristics and genesis of the Miocene intermediate-acid high Sr–Y ratio magmatic rocks in the eastern segment of the gangdise bedrock, Southern Tibet. *China J Petrol.* 35(6):1627–1646 (**in Chinese with English abstract**).
- Xu Q, Zeng L, Zhao L, Hu Z, Wang H, Shen Y, Wang Y, Wang Y (2020) Geochemical characteristics and petrogenesis of Miocene high Sr/Y rocks in Xigatze fore-arc basin, southern Tibet. *Lithos.* 366–367:105543.
- Xu YM, Jiang SY, Zhu JX (2021) Factors controlling the formation of large porphyry Cu deposits: A case study from the Jiurui ore district of Middle-Lower Yangtze River Metallogenic Belt using

- in-situ* zircon and apatite chemistry from syn-mineralization intrusions. *Ore Geol Rev.* 133:104082.
- Yin Q, Lang X, Cui Z, Yan Z, Xie F, Wang X (2016) Geology and Geochemistry constraints on the genesis of The No.2 porphyry copper–gold deposit in the Xiongcun district, Gangdese porphyry copper belt, Tibet, China. *Geol Geochem.* 59(1):32–22.
- Zhang SQ, Mahoney JJ, Mo XX, Ghazi AM, Milani L, Crawford AJ, Guo TY, Zhao ZD (2005) Evidence for a widespread Tethyan upper mantle with Indian-Ocean type isotopic characteristics. *J Petrol.* 46:829–858.
- Zhang H, Zhong KH, Wu H, Yang HR, Li GM, Ma DF (2015) The prospecting direction of porphyry copper deposits related to subduction-collision in gangdise metallogenic belt, Tibet. *Sediment Tethys Geol.* 35(3):88–93 (in Chinese with English abstract).
- Zhang X, Ni P, Wang G, Jiang D, Zhu R, Jiang Y, Wang F (2022) Magmatic controls on the mineralization potential of a porphyry Cu system: the case of Jurassic Tongshan skarn Cu deposit in the Qin-Hang Belt, South China. *Gondwana Res.* 101:203–223.
- Zhang A, Zheng Y, Fu Q, Yang Z, Shen Y (2023) Ore-forming material sources of the Pb–Zn–(Ag–Fe–Cu) deposits in the northern Gangdese belt, Lhasa terrane: constraints from geology, geochemistry and S–Pb isotopes. *Ore Geol Rev.* 159:105491.
- Zhang XB (2020) Origin evolution and geochemistry of Cretaceous granites from the southeastern coast of China. 6:43–51 (in Chinese with English abstract).
- Zhao H (2012) Study on metallogenic regularity of Mesozoic and Cenozoic copper deposits in gangdise metallogenic belt. Master's Chengdu Univ Technol. 6:43–51 (in Chinese with English abstract).
- Zhao Z, Mo X, Dilek Y, Niu Y, DePaolo DJ, Robinson P, Zhu D, Sun C, Dong G, Zhou S, Luo Z, Hou Z (2009) Geochemical and Sr–Nd–Pb–O isotopic compositions of the post-collisional ultrapotassic magmatism in SW Tibet: Petrogenesis and implications for India intra-continental subduction beneath southern Tibet. *Lithos.* 113(1):190–212.
- Zhao J, Qin K, Li G, Li J, Xiao B, Chen L, Yang Y, Li C, Liu Y (2014) Collision-related genesis of the Sharang porphyry molybdenum deposit, Tibet: evidence from zircon U–Pb ages, Re–Os ages and Lu–Hf isotopes. *Ore Geol Rev.* 56:312–326.
- Zhao P, Yuan S, Mao J, Santosh M, Zhang D (2017a) Zircon U–Pb and Hf–O isotopes trace the architecture of polymetallic deposits: a case study of the Jurassic ore-forming porphyries in the Qin-Hang metallogenic belt, China. *Lithos.* 292–293:132–145.
- Zhao XB, Xue CJ, Chi GX, Mo XX, Nurtaev B, Zhang GZ (2017b) Zircon and molybdenite geochronology and geochemistry of the Kalmakyr porphyry Cu–Au deposit, Almalyk district, Uzbekistan: implications for mineralization processes. *Ore Geol Rev.* 86:807–824.
- Zhao X, Yang Z, Zhang S, Yang W, Zheng Y, Wang X, Dou S, Liu H (2022) Miocene adakitic magmatism and conditions of porphyry metallogenesis in the Gangdese magmatic arc, Tibet. *Ore Geol Rev.* 151:105207.
- Zhu DC, Pan GT, Chung SL, Liao ZL, Wang LQ, Li GM (2008) SHRIMP zircon age and geochemical constraints on the origin of lower Jurassic volcanic rocks from the Yeba formation, southern Gangdese, South Tibet. *Int Geol Rev.* 50(5):442–471.
- Zhu DC, Zhao ZD, Pan GT, Lee HY, Kang ZQ, Liao ZL, Wang LQ, Li GM, Dong GC, Liu B (2009) Early cretaceous subduction-related adakite-like rocks of the Gangdese Belt, southern Tibet: products of slab melting and subsequent melt–peridotite interaction? *J Asian Earth Sci.* 34(3):298–309.
- Zhu DC, Mo XX, Niu Y, Zhao ZD, Wang LQ, Liu YS, Wu FY (2009) Geochemical investigation of Early Cretaceous igneous rocks along an east–west traverse throughout the central Lhasa Terrane Tibet. *Chemical Geology.* 268(3–4): 298–312.
- Zhu DC, Zhao ZD, Niu Y, Mo XX, Chung SL, Hou ZQ, Wang LQ, Wu FY (2011) The Lhasa Terrane: Record of a microcontinent and its histories of drift and growth. *Earth Planet Sci Lett.* 301(1):241–255.
- Zhu DC, Zhao ZD, Niu Y, Dilek Y, Hou ZQ, Mo XX (2013) The origin and pre-Cenozoic evolution of the Tibetan Plateau. *Gondwana Res.* 23(4):1429–1454.
- Zhu JJ, Hu R, Bi XW, Hollings P, Zhong H, Gao JF, Pan LC, Huang ML, Wang DZ (2022) Porphyry Cu fertility of eastern Paleo–Tethyan arc magmas: evidence from zircon and apatite compositions. *Lithos.* 424–425:10677.

Springer Nature or its licensor (e.g. a society or other partner) holds exclusive rights to this article under a publishing agreement with the author(s) or other rightsholder(s); author self-archiving of the accepted manuscript version of this article is solely governed by the terms of such publishing agreement and applicable law.